LETTER

Focused-Ion-Beam-Assisted Magnet Fabrication and Manipulation for Magnetic Field Detection Applications

Humberto Campanella,*,† R. P. del Real,‡ Marina Díaz-Michelena,‡ Marta Duch,† Héctor Guerrero,‡ Jaume Esteve,† and José A. Plaza†

Instituto de Microelectrónica de Barcelona (IMB-CNM), CSIC, Campus UAB s/n, 08193 Bellaterra, Barcelona, Spain, and Instituto Nacional de Técnica Aeroespacial (INTA), Carreterra Torrejón-Ajalvir km 4, 28850 Torrejón de Ardoz, Spain

ABSTRACT A focused-ion-beam-assisted technique intended for ultrasmall, hard-magnet fabrication has been developed. By means of ion-beam-induced milling and deposition, reduced-size NdFeB magnets were extracted from a macroscopic quarry and bonded to the surface of a thin-film bulk acoustic resonator (FBAR). Electrical characterization of the FBAR before and after bonding of the magnet was carried out, thus observing both a downshifting of the resonance frequency and a reduction of the quality factor of the resonator. The magnetic behavior of the nanomagnet has been confirmed by means of magnetometry measurements based on atomic force microscopy.

KEYWORDS: hard-magnet nanofabrication • focused ion beam • thin-film bulk acoustic wave resonator

INTRODUCTION

Technological applications and fundamental research on micro- and nanomagnetism have motivated the study of reduced-size magnetic structures. Several techniques and methods for magnetic material manipulation and synthesis at the nanometer scale have been reported (1−3). For example, monodisperse FePt nanoparticles with a size of about 2 nm have been synthesized by means of chemical reduction (4). Also, an implementation of strategies to deposit single-molecule magnets using microcontact printing is reported by Mannini et al. (5). Different lithographic techniques for the fabrication and self-assembly of magnetic nanostructures as data storage media have been implemented so far. The fabrication of 200-nm-period nanomagnet arrays for magnetic information storage using interference lithography and a negative resist (6) and a large area technique based on deep ultraviolet lithography followed by a lift-off process for the fabrication of magnetic $Ni_{80}Fe_{20}$ nanostructures (7) have been developed. A quite different approach is the nanometer-sized magnet fabricated on the tip of a tungsten needle by electron-beam-induced deposition with $Fe(CO)_5$ gas (8). Precisely, one of the biggest technological challenges is how to produce and to place small magnets on another structure. Previous works have explored the combined use of acoustic resonators and soft magnetic materials to detect the magnetic field gradient as well (9−13). Also previously, soft magnetic materials like FePt or Ni compounds have been implemented in the shape of tips or deposited thin films, which are milled to reduce the dimensions of the magnetic material using focused-ion-beam (FIB) techniques. According to this approach, magnetic force microscopy tips have been fabricated (14−17). Another interesting case is the FIB-assisted patterning of magnetic films deposited on microcantilevers for torque magnetometry study (18) and micromechanical oscillators for magnetic detection (19). Although the FIB technique has been used for manipulation of soft magnetic material thin films, no evidence of permanent magnet mechanization utilizing this tool has been reported to date.

In this paper, we describe a FIB-assisted method for extraction and placement of reduced-size magnets on micromachined devices. For an illustration of the technique, we have demonstrated the method by extracting and placing a reduced-size magnet on top of a thin-film bulk acoustic resonator (FBAR) and on the vertex of a silicon cantilever. Magnetometry measurements based on atomic force microscopy (AFM) have also been done to confirm the magnetic behavior of the nanomagnet. Placement of the magnet on the FBAR has been carried out with the aim of magnetic-field detection, taking advantage of the high-frequency sensitivity of FBARs to external loading (20). Compared to previous works, the main contribution of the magnet fabrication technique presented here is such that the obtained micro- or nanomagnet is a hard, rare-earth magnet and not a soft magnetic material, as is done in current art. This would eventually represent an improvement in sensitivity for future magnetic applications because of the good magnetic properties that rare-earth magnets show.

EXPERIMENTS AND DISCUSSION

The process of fabrication and manipulation of the magnet depicted in the schematic of Figure 1 involves (a)

* Phone: +34 93 594 7700. E-mail: hcampane@cnm.es.
Received for review December 1, 2008 and accepted February 5, 2009
† IMB-CNM, CSIC.
‡ INTA. Phone: +34 915 201 183.
DOI: 10.1021/am800205d

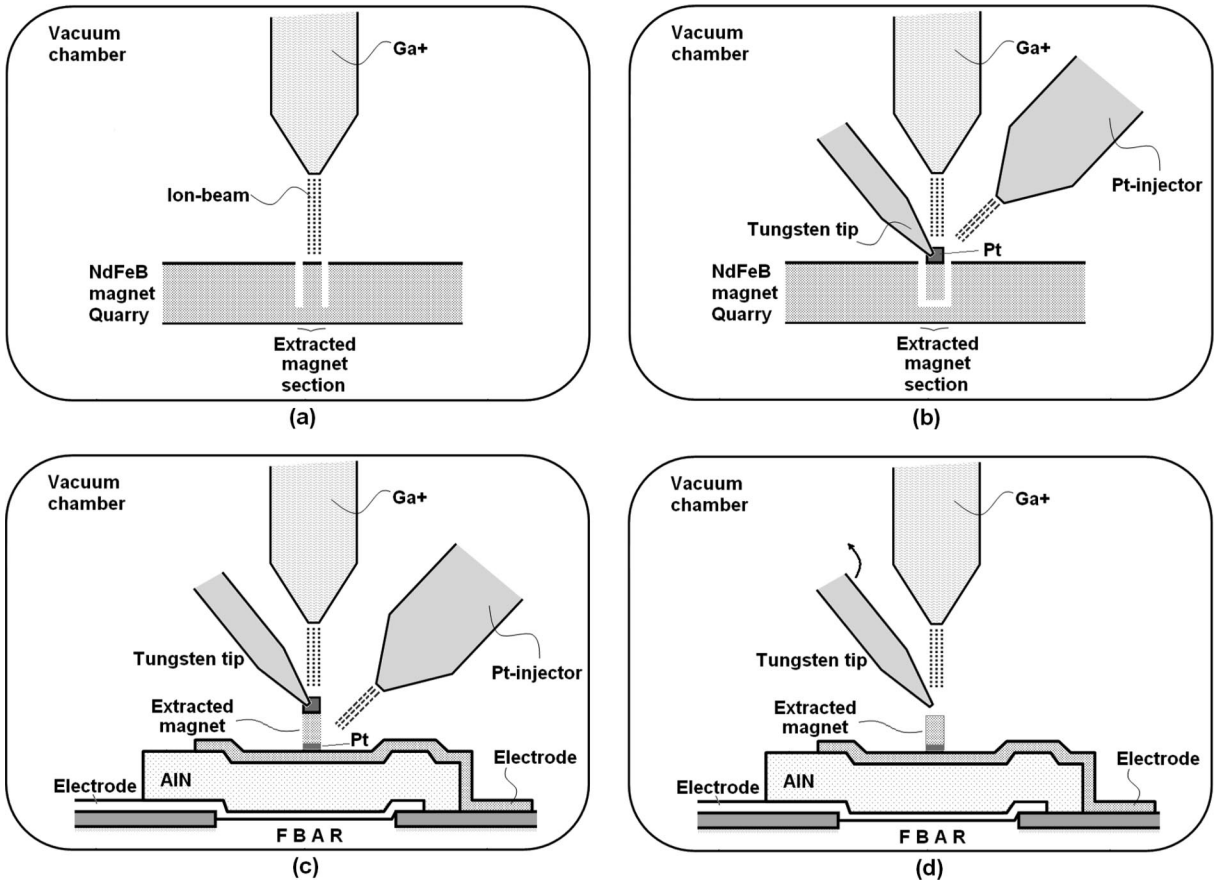

FIGURE 1. Process of extraction and manipulation of the magnet: (a) patterning of the reduced-size magnet and its extraction from the NdFeB quarry; (b) attachment of the magnet to a carrying-and-placing tungsten tip; (c) placement of the magnet on and bonding to the surface of the FBAR; (d) detachment of the magnet and tip.

patterning of the reduced-size magnet and its extraction from a large rare-earth-magnet quarry, (b) attachment of the magnet to a carrying-and-placing tungsten tip, (c) placement of the magnet on and bonding to the surface of the FBAR (or the cantilever), and (d) detachment of the magnet and tip.

First, a millimeter-sized piece of a commercial NdFeB magnet serving as a quarry for the micro- or nanomagnet extraction is placed inside the FIB chamber. Commercial NdFeB magnets are often available in rod-shaped samples of about 2−6 mm in length and diameter; we have used one with a diameter of 2 mm. In order to make the patterning of the nanomagnet easier and to reduce the milling time inside the FIB chamber, a small section of the macroscopic rod was used. This section can be obtained by means of a saw or another mechanical tool. In Figure 2, a semicircular section of a rod-shaped magnet used as a quarry is observed. Accompanying the magnet, a tungsten tip for manipulation and the precursor gas injectors can also be seen.

Patterning of the magnet was performed inside a Carl Zeiss Crossbeam 1560XB FIB, a dual-beam instrument. Gallium ion (Ga^+) beams, accelerated at 30 kV, are able to promote the decomposition of the precursor gas crossing their path, leading to ion-assisted chemical vapor deposition (IACVD) or milling. In our case, a metal−organic precursor containing platinum is injected close to the magnet in the sample chamber of the FIB machine and decomposed by

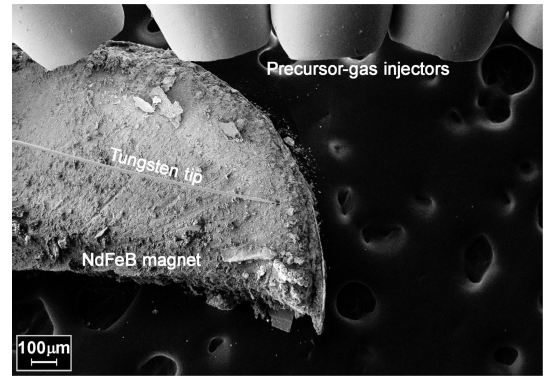

FIGURE 2. Setup of the ultrasmall magnet extraction: the NdFeB millimeter-sized quarry, the precursor gas pipes, and the tungsten tip positioned above the quarry (at left).

the ion beam. This procedure gives rise to milling or localized deposition of an amorphous compound in the area scanned by the beam by carefully adjusting the dwell time, positioning, and current density of the ion beam. This compound, according to Auger electron spectroscopy measurements, contains carbon (65%), platinum (27%), and gallium (8%), with its mass density being estimated to be 4 g/cm^3 (21).

The magnet patterning begins marking the quarry with the ion beam in order to ease the search for the patterned area. The markings are cross-shaped patterns that can be recognized by the control system of the FIB and are useful for locating the working site because of the long milling times

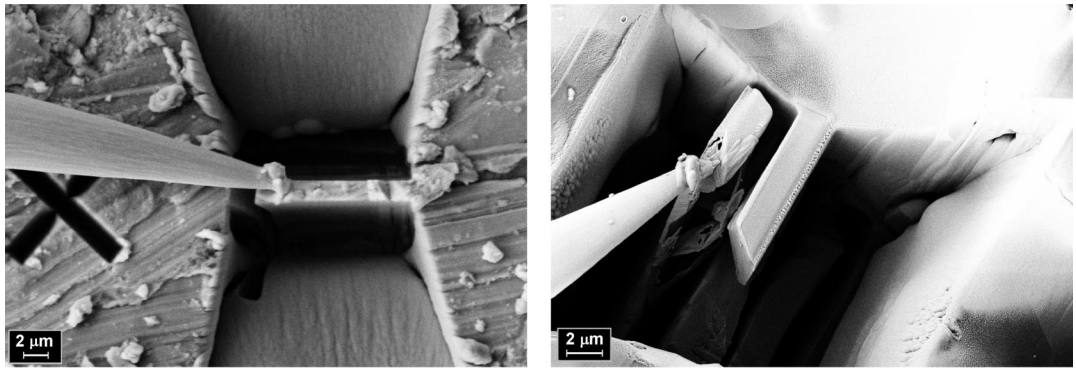

(a) (b)

FIGURE 3. FIB-assisted ultrasmall magnet patterning and extraction. (a) The tungsten tip is bonded to the parallelepiped patterned on the quarry (the marking cross pattern at left allows for searching of the quarry). (b) A piece of the quarry is separated from the quarry. Patterning and bonding are performed by ion-beam-assisted milling and deposition, respectively.

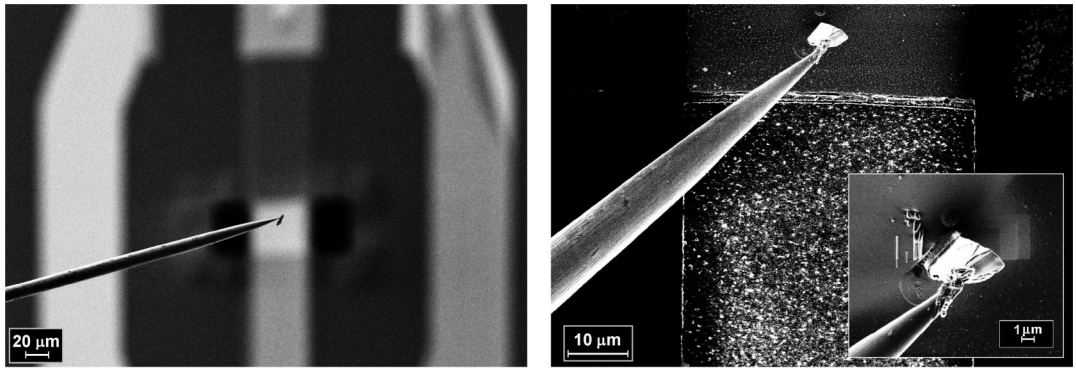

(a) (b)

FIGURE 4. Placement of the ultrasmall magnet on a FBAR: (a) magnet located several hundreds of micrometers above the FBAR; (b) tungsten tip with the magnet when the FBAR's electrode is approached. Inset: The magnet is being bonded to the surface of the electrode by means of Pt/C/Ga compound deposition.

required to generate the quarry, typically hours. First, the region around the quarry is milled to allow extraction of a small, rectangular-shaped piece of the magnet. After milling of an area of squared micrometers, a parallelepiped-like volume with one of its faces still attached to the quarry was formed. Its surface parallel to the surface quarry was about 2 μm × 10 μm. This parallelepiped of size 1 μm × 2 μm × 10 μm will become the micro- or nanomagnet after further processing and release from the big magnet. At this point, a tungsten tip handled with a stage of the FIB is bonded to the parallelepiped by means of IACVD, with the deposited platinum compound soldering the tip and the magnet at their contact surfaces. The region around the quarry, the marking cross pattern, the parallelepiped still attached to the magnet, and the tungsten tip bonded to it are shown in the scanning electron microscopy (SEM) image of Figure 3a. A gap of about 2 μm at the left side of the parallelepiped can be observed. This gap is obtained after milling of the parallelepiped, in order to allow extraction of the magnet (in addition to an ion-based "cut" from the base of the parallelepiped). After release of the small magnet, careful manipulation is needed to compensate for the magnetic attraction/repulsion forces to the quarry in the short distances. In the SEM image of Figure 3b, the extracted magnet stuck to the quarry is observed. Rough moving of the tip may arise in detachment of the magnet; thus, stepped movement of the tip is preferred.

The process continues with the placement and bonding of the magnet on the surface of the FBAR. For this purpose, the magnet is located at the target position on the FBAR electrode, as shown in Figure 4a,b, and bonded with Pt/C/Ga using the ion beam (the soldered magnet in the inset). Alignment of the ion beam with the appropriate axis is carried out to ensure contact of the deposited compound and the lower and upper surfaces of the magnet and electrode, respectively. Once the magnet is bonded, this is separated from the tungsten tip. Ion-beam-assisted milling of the platinum compound in between the tip and the magnet eliminates the tying material, thus releasing the stage with the tip. Finally, the tip is moved away and the magnet is attached to the FBAR, as observed in the SEM images of parts a and b of Figure 5, respectively (a magnified view of the magnet can be seen in the inset of Figure 5b).

The high density of NdFeB, 7500 kg/m^3, and the mass of the magnet allow it to be a strong influence on the resonance frequency and quality factor of the FBAR. Because of the mass-loading effect, downshifting in the resonance frequency of the resonator occurs. The plots of Figure 6a compare experimental measurements of the reflection scattering parameter (S11) of the FBAR before and after attach-

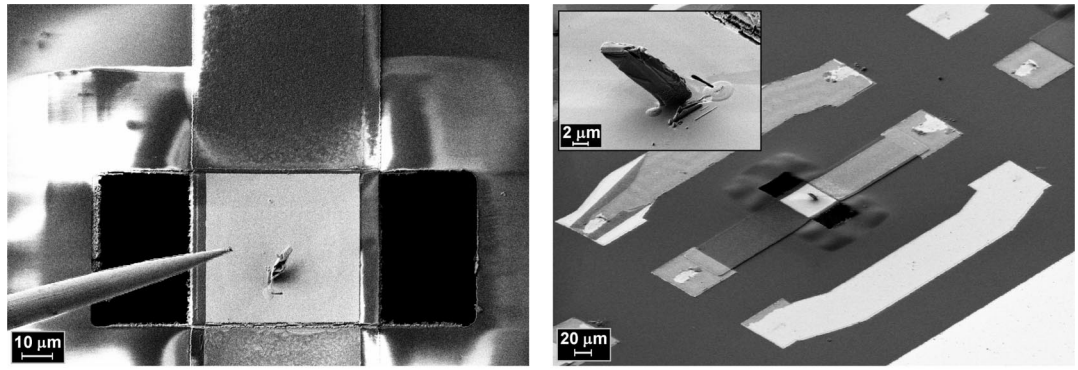

FIGURE 5. Magnet placed on the FBAR: (a) detail of the electrode with the magnet and tip moving away once separated from the magnet; (b) overview of the FBAR, embedded on a resonance-frequency coplanar test structure (the deposited magnet is magnified in the inset).

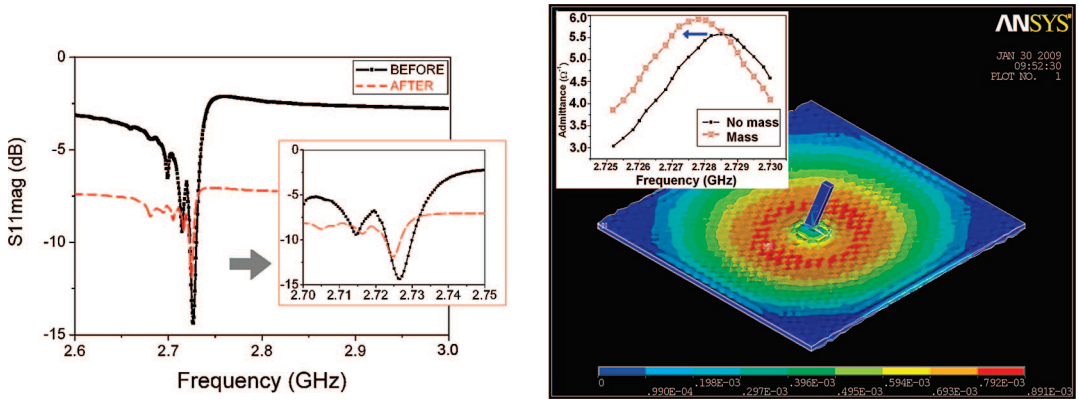

FIGURE 6. Characterization of the FBAR's frequency response, before and after the ultrasmall magnet bonding: (a) Experimental measurement of the reflection scattering parameter S11. Downshifting of 1.6 MHz and a 75% quality factor reduction of the resonance frequency demonstrate the successful attachment and mechanical coupling between the magnet and resonator (inset: zoom-in around the resonance frequency). (b) FEM of the FBAR with a deposited magnet (frequency responses around the resonance frequencies). The mode shaping is modified because of the mass-loading effect of the magnet. The frequency shifting is of the same magnitude as that of the experimental setup.

ment of the magnet. As observed, the resonance frequency shifts down about 1.6 MHz and the size of the resonance peak is reduced. In the same way, the harmonic analysis of the finite element model (FEM) of the FBAR-and-magnet ensemble shown in Figure 6b also revealed a downshifting of the resonance frequency comparable to that of the experimental characterization (the FBAR frequency responses before and after the magnet's deposition are shown in the inset of the figure). The mode shaping allows us to see how the nanomagnet deposition creates a mass-loading effect, which deforms the contour of the FBAR's surface when it resonates. The lower size of the resonance is related to a reduction of the quality factor (Q) of the resonator. Thus, both the unloaded and magnet-loaded Q factors have been calculated. Before the magnet was bonded, the FBAR exhibited a Q factor of 525, but once the magnet is bonded, and upon these curves, the new Q factor is 135, which means a reduction of 75%. This drastic reduction of the Q factor is attributed to the high mass, in the range of $(1-2) \times 10^{-10}$ g, and aspect ratio of the magnet, thus leading to a mass responsivity between 2 and 10×10^{-17} g/Hz. According to previous work, this amount of mass saturates the resonant behavior of the FBAR for localized mass deposition (20). Both aspects are to be considered during the design of a magnetic field detection application of this technique. The main idea of the detector is that the micro/nanomagnet is attracted to the magnetic field source when placed on the FBAR and immersed on a magnetic field gradient generated by an external influence or particle. This attraction force would add stress to the acoustic layer of the FBAR, changing its resonance frequency.

On the other hand, a second parallelepiped-shaped magnet was deposited on the vertex of a silicon cantilever of dimensions $800 \times 30 \times 1.5\ \mu m^3$, as shown in the SEM image of Figure 7. AFM-based magnetometry measurements were performed to evaluate the magnetic properties of the magnet. By means of a current source, a coil, and an AFM, deformation of the cantilever of about 3.5 nm was detected by the photodiode array of the AFM. According to the coil's magnetic gradient calibration, assuming a NdFeB theoretical magnetization $M = 8.0 \times 10^5$ A/m (equivalent to a magnetic polarization $J = 1$ T), the cantilever's spring constant $k = 8.2 \times 10^{-3}$, and the estimated magnet's deposition angle (45°), the experimental value of M was extracted to be 2.1×10^5 A/m (equivalent to $J = 0.264$ T). This value is on the same order of magnitude as the theoretical M of the source NdFeB and confirms the magnetic behavior of the small magnet. Differences between the expected and obtained values of M may be explained by the difficulties in accurately determining the coil-to-magnet distance, the deposition

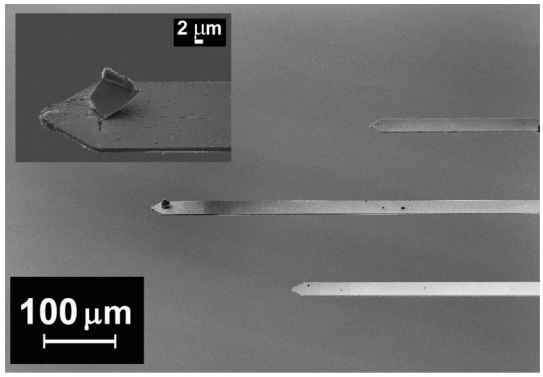

FIGURE 7. Parallelepiped-shaped magnet deposited on the vertex of a silicon cantilever of dimensions 800 × 30 × 1.5 μm^3.

angle and dimensions of the magnet, and/or the ion-beam radiation effects on the magnetic properties of the extracted piece. Concerning this point, previous experiments have demonstrated that the FIB-assisted nanofabrication has no effect on the *Q* factor and the electrical performance of the FBAR (22). Still, this issue is to be further developed in future work.

CONCLUSIONS

We have presented a FIB technique for micro- and nanomagnet fabrication and manipulation. The technique involves milling of a magnet quarry and ion-beam-assisted deposition of a bonding compound in order to extract the nanomagnet and to attach it to a microelectromechanical system structure. Future development of the technique will involve a further reduction of the magnet size and tailoring of its aspect ratio to optimize the manipulation and maximize the quality factor. This technique could open some research lines on the magnetic field detection. The dimensions of the magnetic samples do not allow their full characterization by means of standard vibrating sample magnetometry or alternating gradient magnetometry (AGM). Therefore, this technique itself could lead to the development of new μAGMs with improved sensitivity. In this way, evaluation of the magnetization axis of the extracted magnet would contribute to the refinement of both the extraction technique and placement of the magnet on the FBAR in order to maximize the magnetic sensor's performance.

Acknowledgment. The authors thank Jordi Llobet and Xavier Borrisé at IMB-CNM (CSIC) for FIB support and operation. This work is funded by the INTA, under industrial research collaboration in the context of MICINN Project OPTOMAG-MANTIS (ESP-2005-05278). Partial support has been provided by the MINAHE 2 project (MEC-TEC2005-07996-CO2-01).

REFERENCES AND NOTES

(1) Monnier, V.; Delalande, M.; Bayle-Guillemaud, P.; Samson, Y.; Reiss, P. *Small* **2008**, *4* (8), 1139–1142.
(2) Terris, B. D.; Thomson, T. *J. Phys. D: Appl. Phys.* **2005**, *38* (12), R199–R222.
(3) Cugat, O., Reyne, G., Delamare J., Eds. *Magnetic Microsystems: Mag-MEMS*; ISTE Publishing Co.: London, 2007.
(4) Elkins, K. E.; Vedantam, T. S.; Liu, J. P.; Zeng, H.; Sun, S.; Ding, Y.; Wang, Z. L. *Nano Lett.* **2003**, *3* (12), 1647–1649.
(5) Mannini, M.; Bonacchi, D.; Zobbi, L.; Piras, F. M.; Speets, E. A.; Caneschi, A.; Cornia, A.; Magnani, A.; Ravoo, B. J.; Reinhoudt, D. N.; Sessoli, R.; Gatteschi, D. *Nano Lett.* **2005**, *5* (7), 1435–1438.
(6) Farhoud, M.; Ferrera, J.; Lochtefeld, A. J.; Murphy, T. E.; Schattenburg, M. L.; Carter, J.; Ross, C. A.; Smith, H. I. *43rd International Conference on Electron, Ion, and Photon Beam Technology and Nanofabrication*, Marco Island, FL, June 1−4, 1999; American Institute of Physics: Melville, NY, 1999; pp 3182−3185.
(7) Singh, N.; Goolaup, S.; Adeyeye, A. O. *Nanotechnology* **2004**, *15* (11), 1539–1544.
(8) Takeguchi, M.; Shimojo, M.; Che, R.; Furuya, K. *J. Mater. Sci.* **2006**, *41* (9), 2627–2630.
(9) Maglione, M.; Zhu, W.; Wang, Z. H. *Appl. Phys. Lett.* **2005**, *87* (9), 092904–3.
(10) Pan, D. A.; Bai, Y.; Volinsky, A. A.; Chu, W. Y.; Qiao, L. J. *Appl. Phys. Lett.* **2008**, *92* (5), 052904–3.
(11) Dong, S.; Zhai, J.; Li, J.; Viehland, D. *Appl. Phys. Lett.* **2006**, *88* (8), 082907–2.
(12) Maya, L.; Thundat, T.; Thompson, J. R.; Stevenson, R. J. *Appl. Phys. Lett.* **1995**, *67* (20), 3034–3036.
(13) Heh, S. J.; Lin, K. D.; Jein, Y. M.; King, F. D.; Lee, F. L.; Chin, T. S. *IEEE Trans. Magn.* **1990**, *26* (5), 2637–2639.
(14) Phillips, G. N.; Siekman, M.; Abelmann, L.; Lodder, J. C. *Appl. Phys. Lett.* **2002**, *81* (5), 865–867.
(15) Liu, Z.; Dan, Y.; Jinjun, Q.; Wu, Y. *J. Appl. Phys.* **2002**, *91* (10), 8843–8845.
(16) Gao, L.; Yue, L. P.; Yokota, T.; Skomski, R.; Liou, S. H.; Takahoshi, H.; Saito, H.; Ishio, S. *IEEE Trans. Magn.* **2004**, *40* (4), 2194–2196.
(17) Schreiber, S.; Savla, M.; Pelekhov, D. V.; Iscru, D. F.; Selcu, C.; Hammel, P. C.; Agarwal, G. *Small* **2008**, *4* (2), 270–278.
(18) Yuan, L.; Gao, L.; Sabirianov, R.; Liou, S. H.; Chabot, M. D.; Min, D. H.; Moreland, J.; Han, B. *IEEE International Magnetics Conference INTERMAG 2006*; IEEE: New York, 2006; p 583.
(19) Chabot, M. D.; Moreland, J. M.; Lan, G.; Sy-Hwang, L.; Miller, C. W. *J. Microelectromech. Syst.* **2005**, *14* (5), 1118–1126.
(20) Campanella, H.; Esteve, J.; Montserrat, J.; Uranga, A.; Abadal, G.; Barniol, N.; Romano-Rodriguez, A. *Appl. Phys. Lett.* **2006**, *89* (3), 033507–3.
(21) Vilà, A.; Hernández-Ramírez, F.; Rodríguez, J.; Casals, O.; Romano-Rodríguez, A.; Morante, J. R.; Abid, M. *Mater. Sci. Eng., C* **2006**, *26*, 1063–1066.
(22) Campanella, H.; Hernández-Ramírez, F.; Romano-Rodríguez, A.; Montserrat, J.; Uranga, A.; Barniol, N.; Esteve, J. *J. Micromech. Microeng.* **2007**, *17*, 2380–2389.

AM800205D